Impaired dynamic cerebrovascular response to hypercapnia predicts development of white matter hyperintensities

Kevin Sam[a,b], John Conklin[b], Kenneth R. Holmes[c], Olivia Sobczyk[c], Julien Poublanc[b], Adrian P. Crawley[b], Daniel M. Mandell[b], Lakshmikumar Venkatraghavan[d], James Duffin[a,d], Joseph A. Fisher[a,c,d], Sandra E. Black[e,1], David J. Mikulis[b,*,1]

[a] Department of Physiology, The University of Toronto, Toronto, ON, Canada
[b] Division of Neuroradiology, Joint Department of Medical Imaging, University Health Network, Toronto, ON, Canada
[c] Institute of Medical Sciences, The University of Toronto, Toronto, ON, Canada
[d] Department of Anaesthesia, University Health Network, Toronto, ON, Canada
[e] L.C. Campbell Cognitive Neurology Research Unit, Sunnybrook Health Sciences Centre, Toronto, ON, Canada

ARTICLE INFO

ABSTRACT

Purpose: To evaluate the relationship between both dynamic and steady-state measures of cerebrovascular reactivity (CVR) and the progression of age-related white matter disease.
Methods: Blood oxygen level-dependent (BOLD) MRI CVR scans were acquired from forty-five subjects (age range: 50–90 years, 25 males) with moderate to severe white matter disease, at baseline and one-year follow-up. To calculate the dynamic (τ) and steady-state (ssCVR) components of the BOLD signal response, the $P_{ET}CO_2$ signal waveform was convolved with an exponential decay function. The τ corresponding to the best fit between the convolved $P_{ET}CO_2$ and BOLD signal defined the speed of response, and the slope of the regression between the convolved $P_{ET}CO_2$ and BOLD signal defined ssCVR. ssCVR and τ were compared between normal-appearing white matter (NAWM) that remains stable over time and NAWM that progresses to white matter hyperintensities (WMHs).
Results: In comparison to contralateral NAWM, NAWM that progressed to WMH had significantly lower ssCVR values by mean (SD) 46.5 (7.6)%, and higher τ values by 31.9 (9.6)% (both $P < 0.01$).
Conclusions: Vascular impairment in regions of NAWM that progresses to WMH consists not only of decreased magnitude of ssCVR, but also a pathological decrease in the speed of vascular response. These findings support the association between cerebrovascular dysregulation and the development of WMH.

1. Introduction

In elderly individuals, magnetic resonance imaging (MRI) of cerebral white matter frequently shows patchy or confluent hyperintensity on T2-weighted images, termed "white matter hyperintensities" (WMHs) if they are of presumed vascular origin (Wardlaw et al., 2013). WMHs occur predominantly in the periventricular white matter, particularly around the horns of the lateral ventricles and in the centrum semiovale. Population-based studies show the prevalence of WMHs on MRI in elderly people to be 62–95% (Liao et al., 1997; Launer et al., 2006).

Given this high prevalence in normally functioning elderly individuals, WMHs were initially considered benign. However, subsequent research showed that WMHs are associated with disability (Whitman et al., 2001; Blahak et al., 2009), cognitive decline (Verdelho et al., 2010), and progression to dementia (Schmidt et al., 2002; Gunning-Dixon and Raz, 2000). Nevertheless, the detailed pathophysiology of WMH progression remains poorly understood, and is the subject of this investigation.

The mechanisms leading to WMHs are complex. Age-related stenosis and hypoperfusion of medullary arterioles may cause low grade ischemic injury to deep white matter. In addition, impaired vascular autoregulation may contribute to the progression of WMHs in areas that are not well capillarized, predisposing white matter to hypoperfusion injury. Uh et al. (2010) found a reduction in both cerebrovascular reactivity (CVR) and cerebral blood flow (CBF) in regions of WMH compared to normal-appearing white matter (NAWM). They also noted that areas of WMH were characterized by significant blood-brain barrier leakage and abnormal diffusion MRI metrics.

---

* Corresponding author at: Toronto Western Hospital, Joint Department of Medical Imaging, McLaughlin Pavilion, 3rd Floor Room 431, 399 Bathurst St., Toronto, ON M5T 2S8, Canada.
E-mail address: mikulis@uhnres.utoronto.ca (D.J. Mikulis).
[1] Please note that Drs. Sandra E. Black and David J. Mikulis wish to be listed as co-senior authors.

CVR is defined as the change in blood flow in response to a vasoactive stimulus. We have established a quantitative approach to measuring CVR using blood oxygen level-dependent (BOLD) MRI as a surrogate for blood flow and controlling the end-tidal partial pressures of carbon dioxide ($P_{ET}CO_2$) and oxygen ($P_{ET}O_2$) to provide a standardized vasoactive stimulus (Spano et al., 2013). By applying a square wave change in $P_{ET}CO_2$ during BOLD imaging, we are able to parse CVR into two different metrics: 1) steady-state component of CVR (ssCVR), which occurs after the vasodilatory response to the CO_2 stimulus is complete. Mathematically, it is the asymptote of the exponential rise in the BOLD signal in response to a rapid (step change) in arterial PCO_2 and 2) Tau (τ), which represents the rate constant of this exponential and is a metric indicating how rapidly a vascular bed can respond to a step change in PCO_2. It is of physiological interest as it is an indicator of vascular compliance (Poublanc et al., 2015).

We measured these metrics in areas of WMH as well as in NAWM that progress to WMH on follow-up imaging, with particular attention to the speed of the vascular response. Supporting this approach is a recent study that found that the cerebral deep white matter has prolonged τ and reduced ssCVR compared to grey matter (Poublanc et al., 2015). We hypothesized that reduced ssCVR and prolonged τ would occur in WMHs as well as NAWM that progressed to WMH with time, when compared to NAWM that did not progress to WMH.

2. Methods

2.1. Subject recruitment and assessment

This prospective bi-centric study examined elderly subjects with moderate to severe WMH at two time points set one year apart (baseline and follow-up). This study conformed to the standards set by the latest revision of the Declaration of Helsinki and was approved by the Research Ethics Board of the University Health Network and Research Ethics Board of Sunnybrook Health Sciences Centre. Written informed consent was obtained from all participants. Subjects were recruited from outpatient neurology clinics at Toronto Western Hospital (TWH) and Sunnybrook Health Sciences Centre (SHSC). Magnetic resonance angiography (MRA) or computed tomography angiography (CTA) and T2-weighted fluid-attenuated inversion recovery (FLAIR) images of all patients were screened by experienced neuroradiologists (D.J.M. & D.M.M.). Subjects were enrolled based on the following inclusion criteria: (1) no recent white matter infarct (patients were excluded if they had a previous DWI positive white matter infarct within the 3 months preceding study enrolment); (2) no prior cortical infarct >2 cm or cavitary white matter lesion >2 cm; (3) over the age of 50; (4) MRI white matter disease burden ≥ Fazekas Grade 2; (5) no hemodynamically significant (i.e., >50%) ICA or vertebrobasilar stenosis on CTA or MRA; (6) no evidence of dissection; (7) no history of pulmonary or cardio-embolic disease.

Subjects with motion artifacts on BOLD images were excluded. Forty-five subjects (age range, 50 to 91 years; 25 males and 20 females) with moderate to severe WMHs met the inclusion criteria and were considered in the subsequent analysis (see Table 1 for subject characteristics).

2.2. Image acquisition

Subjects underwent MRI scans on either a 3-Tesla GE system (Signa HDx platform, GE Healthcare, Milwaukee, Wis) or a 3-Tesla Philips Achieva system (Philips Medical Systems, Best, Netherlands) using an eight-channel phased array head coil. Subjects were asked to refrain from heavy exercise and drinking alcohol or caffeine on the day of each scan. The image acquisition parameters were as follows, with values provided for SHSC/TWH: T1-weighted 3D spoiled gradient echo sequence [slice thickness = 1.2 mm (SHSC)/1.5 mm (TWH); no interslice gap; matrix size = 256 × 256; field of view = 22 × 22 cm;

Table 1
Baseline characteristics of subjects. Abbreviations: MoCA = Montreal Cognitive Assessment; WMH = white matter hyperintensities.

Parameter	Value (total $n = 45$)
Demographics	
Age, in years, mean (SD)	74 (9.4)
Men, n (%)	25 (56)
Baseline WMH volume, ccs (SD)	32 (25)
MoCA, mean (SD), 6 missing values	25 (4)
Vascular risk factors, n (%)	
Ischemic stroke	12 (27)
Transient ischemic attack	6 (13)
Coronary artery disease	7 (16)
Hypertension	23 (51)
Hypercholesterolemia	19 (42)
Diabetes mellitus	3 (7)
Current smoking	3 (7)
Obstructive sleep apnea	5 (11)

nominal voxel size = 0.85 × 0.85 × 1.2/0.85 × 0.85 × 1.5 mm; flip angle = 8 / 20°; TE = 2.3/3 ms; TR = 7.8/9.5 ms] and BOLD fMRI using a T2*-weighted echoplanar imaging gradient echo sequence [slice thickness = 3.0/5.0 mm; field of view = 24 × 24 cm; matrix size = 64 × 64; nominal voxel size = 3.75 × 3.75 × 3/3.75 × 3.75 × 5 mm; flip angle = 85/90°; TE = 30 ms; TR = 2000 ms].

2.3. CVR measurement

CVR is defined as the change in blood flow in response to a vasoactive stimulus. BOLD MRI was used as a surrogate of blood flow (Poublanc et al., 2015; Sobczyk et al., 2015; Sam et al., 2015), and an abrupt step increase in the end-tidal partial pressure of carbon dioxide ($P_{ET}CO_2$) was used as the vasoactive stimulus (Han et al., 2011). CVR was calculated as % change in BOLD/Δ $P_{ET}CO_2$, and a color scale ranging from blue to red was used to identify the magnitude of CVR. Negative CVR values were represented in shades of blue, and positive CVR values were represented as shades of yellow, orange, and red.

2.4. Vasodilatory stimulus (gas manipulation, end-tidal pCO$_2$ and pO$_2$ manipulation)

Control of end-tidal partial pressures of carbon dioxide and oxygen ($P_{ET}O_2$) was achieved using an automated gas blender that adjusts the gas composition and flow to a sequential gas delivery breathing circuit (RespirAct™, Thornhill Research Inc., Toronto, Canada) as previously described (Slessarev et al., 2007; Fierstra et al., 2013). The $P_{ET}CO_2$ sequence used during BOLD measurements was 40 mmHg for 60 s (normocapnia), followed by an abrupt hypercapnic step change to $P_{ET}CO_2$ of 50 mmHg for 90 s, a return to baseline for 90 s, a second hypercapnic step change for 120 s, and a return to baseline (Poublanc et al., 2015). Normoxia ($P_{ET}O_2$ ~110 mmHg) was maintained throughout.

2.5. Generating steady-state CVR and τ maps

$P_{ET}CO_2$ was first synchronized with the whole brain average BOLD signal using MATLAB software (Mathworks, Natick, Massachusetts, USA) to compensate for delays in breath sampling and blood flow transit time from the pulmonary to the cerebral circulation. BOLD responses were parsed into steady-state (ssCVR) and dynamic (τ) components using a convolved $P_{ET}CO_2$ stimulus instead of the measured $P_{ET}CO_2$, as previously described (Poublanc et al., 2015). Briefly, the BOLD response was modeled as the $P_{ET}CO_2$ convolved with an exponential decay function [$\exp(-t/\tau)$] representing the hemodynamic response, where t is time and τ is the time constant of the vascular response. τ was allowed to vary from 2 to 100 s in 2 s increments, giving rise to 50 convolved signals. The τ of the convolved $P_{ET}CO_2$ with the highest Pearson correlation

coefficient with the BOLD response was taken as a measure of the speed of response for that particular voxel. ssCVR was calculated as the slope of the regression between the BOLD response and the convolved $P_{ET}CO_2$ waveform that provided the highest Pearson correlation (Poublanc et al., 2015). ssCVR values were expressed as percent MR signal change per mmHg of $P_{ET}CO_2$, whereas τ is measured in seconds. Representative maps of ssCVR, and τ are shown in Fig. 1.

2.6. Generating ROIs of WMH and NAWM

Segmentation of baseline WMH was performed using the Lesion Explorer processing pipeline (Ramirez et al., 2011, 2014). To identify novel WMH on follow-up, the baseline WMH segmentation was overlaid onto follow-up FLAIR, proton density (PD), and T2-weighted images. Evidence of novel WMH on all three image series was required for a lesion to be classified as newly developed WMH. Such lesions were then manually segmented using AFNI (Cox, 1996). T1-weighted anatomical images were segmented into cerebrospinal fluid, grey matter, and white matter using SPM8 (Wellcome Department of Imaging Neuroscience, Institute of Neurology, University College, London, UK). A diamond shaped structuring element was used to erode the white matter ROI in five iterations at the resolution of the T1-weighted image to prevent partial volume effects. The WMH ROI was then subtracted from the eroded WM ROI to give rise to an ROI containing only NAWM.

2.7. Accounting for the confounding factor of spatial location

One important confound in our study is the spatial error associated with each metric due to spatial location; e.g. periventricular CVR may be less than that in white matter near the cortical surface. To account for possible spatial error of the MRI metrics, T1-weighted images were transformed into Montreal Neurological Institute space using SPM8. This transformation matrix was then applied to other MRI metrics, transforming these maps to a standard space but retaining their native structure. Finally, a second ROI of the NAWM was generated that is contralateral and spatially homologous to WMH (Fig. 2).

2.8. Statistical analyses

MRI metrics were compared for the following four ROIs:

1) grey matter;
2) pre-existing WMH;
3) all NAWM; and
4) the subset of NAWM voxels that progressed to WMH on the follow-up scan.

All statistical comparisons were based on a within-subject repeated measures design, which accounted for between-subject differences. Comparison of ssCVR between ROIs was performed using Friedman's test with Dunn's correction for multiple comparisons. Comparison of τ between ROIs was performed using repeated measures one-way
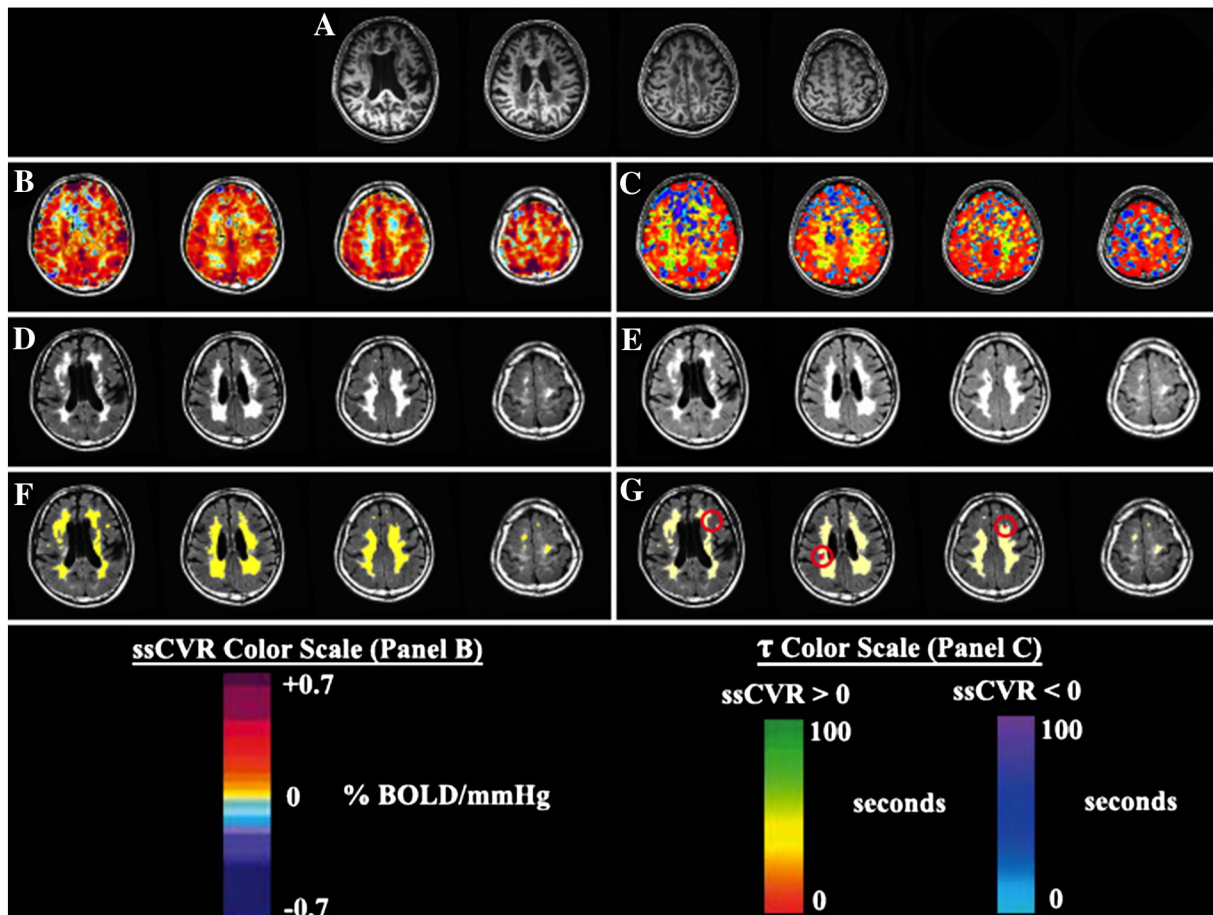

Fig. 1. CVR metrics used to characterize future WMHs. (A) T1-weighted images from a subject with diffuse periventricular and deep WMHs. (B) Steady-state CVR (ssCVR) map in the same subject showing reduced CVR in areas of WMHs. (C) Tau map demonstrating slower vascular responses to carbon dioxide in regions of WMHs. (D) FLAIR images showing WMHs on the baseline scan. Two color scales are used to represent regions with positive ssCVR (red to green) and negative ssCVR (light blue to purple). (E) FLAIR images showing WMHs on the follow-up scan. (F) WMHs identified on the baseline scan are highlighted in yellow. (G) WMHs identified on baseline are highlighted in yellow whereas new hyperintensities identified on follow-up are highlighted in red. CVR values are in units of % BOLD/mmHg. (For interpretation of the references to color in this figure legend, the reader is referred to the web version of this article.)
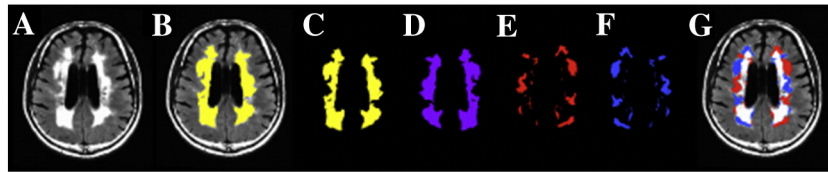
Fig. 2. ROIs used in the comparison of NAWM and hyperintensities considering the confounding spatial factor. (A) FLAIR images from a subject with diffuse periventricular and deep WMHs. (B) WMHs are highlighted in yellow and overlaid on a FLAIR image. (C) WMHs without the underlying FLAIR map. (D) Image C is left-right flipped about the y-axis in MNI coordinates while retaining native structure. (E) Image D is subtracted from Image C, giving rise to NAWM that is contralateral to hyperintensities. (F) Image E is left-right flipped about the y-axis to give rise to the original WMH mask; however, only voxels with contralateral NAWM remain. (G) The final NAWM mask (image E) and WMH mask (image F) used in the characterization of CVR metrics are overlaid on FLAIR images. (For interpretation of the references to color in this figure legend, the reader is referred to the web version of this article.)

ANOVA, with τ as the dependent variable and the various ROIs as the matched-pairs independent variable. Bonferroni corrections for multiple comparisons were made and significance was assumed as $P < 0.05 / (6$ comparisons$) = 0.008$. Mauchly's test was used to detect significant departures from sphericity and degrees of freedom were adjusted using the Greenhouse–Geisser or Huynh-Feldt correction as appropriate. When controlling for differences due to spatial location, comparisons were also made between WMHs and contralateral homologous NAWM using either Wilcoxon matched-pairs signed ranks test (for CVR and ssCVR measurements) or two-tailed paired t-tests (for τ measurements). Statistical significance was assessed with $\alpha = 0.001$.

3. Results

Forty-five subjects (age range: 50–90 years, 25 males) with moderate to severe WMHs participated in this study. Reasons for referral to the memory or stroke prevention clinic included chronic imbalance and headaches, memory impairment, cognitive decline, transient episodes of paresthesia, or syncopal episodes. These subjects had a mean (SD) WMH volume of 26.7 (23.5) mLs per subject at baseline (mean age: 73.1 years), an average WMH volume of 30.0 (25.1) mLs per subject on one-year follow-up, and a WMH progression rate of 0.66 (0.60) mLs/year.

The mean (SD) for each cerebrovascular metric in each group is summarized in Table 2. ssCVR and τ for grey matter were significantly different ($P < 0.01$) from those in all other groups (NAWM, pre-existing WMH, and NAWM that progressed to WMH). All metrics for NAWM were significantly different from those in all other groups. NAWM that progressed to WMH on follow-up had lower ssCVR [0.086 (0.076) vs. 0.172 (0.056) %BOLD/mmHg] and longer τ values [46.02 (15.86) vs. 35.62 (9.30) seconds] compared to NAWM that did not progress to WMHs ($P < 0.01$).

The time constant τ was longer in pre-existing WMH compared to NAWM that did not progress to WMHs [50.25 (11.52) vs. 35.62 (9.30) seconds, $P < 0.001$]. Using spatially corrected regions, this difference was reduced but remained significant [36.95 (7.59) seconds for WMH vs. 34.72 (8.01) seconds for NAWM, $P < 0.001$] (Table 3). Differences in CVR metrics between pre-existing WMH and NAWM that progressed to WMH compared to NAWM that did not progress to WMHs are illustrated in Fig. 3.

4. Discussion

This is the first report of prolonged vascular response times in NAWM that subsequently progresses to WMH. Neither ssCVR, which represents the time-independent magnitude of the BOLD response to a square-wave vasodilatory stimulus, nor τ, which measures the speed of the vasodilatory response, have been measured previously in the context of age-related white matter disease. Our findings therefore support the hypothesis that chronic hypoperfusion plays a role in the development of WMHs. Unlike the richly collateralized cortex, white matter is vulnerable to the development of WMHs because it is perfused by long penetrating medullary end-arteries with poor collateralization. This vascular architecture provides little protection from ischemia during periods of generalized vasodilatation, where blood flow is redirected to areas of preserved vasodilatory capacity (Roman, 1987; Mandell et al., 2008; Sobczyk et al., 2014). The CVR findings are consistent with a prior report by Uh et al. (2010) who found that CVR in WMHs was approximately half of that in NAWM.

The reduced CVR in NAWM that progressed to WMH we found may provide a resolution of the conflicting evidence supporting hypoperfusion as a mechanism for the pathogenesis of WMHs. While several studies have demonstrated reduced CBF in WMHs (Ishii et al., 1986; Fazekas et al., 1988), it is nevertheless unclear whether hypoperfusion is a causative factor for WMHs or a secondary response to the reduced metabolic activity of leukoaraiotic tissue. Our results demonstrate that reductions in ssCVR in NAWM regions *precede* the development of WMHs, suggesting that hemodynamic impairment may be an etiological factor.

Previous studies have looked at vascular response times. The cerebral pial vessels in cats respond to changes in pH rapidly, within approximately 10 s (Greensburg and Reivich, 1977). Previous studies in humans using inhalation of carbogen found that 5 min was required to reach peak flow values as measured by a N_2O washout method (Shapiro et al., 1965). However, this is also the approximate time course for change in arterial PCO_2 after the administration of carbogen (Fisher, 2016) so a faster peak response time could not have been detected. In contrast, our study measured the vascular dynamics in the WM with a change in $P_{ET}CO_2$ within one to two breaths allowing the detection of vascular response times as brief as 10 s (i.e. 2 breaths).

Our finding of slowed vascular responses in NAWM that progresses to WMH is consistent with observations of the penumbra of large infarcts (Englund, 2002), where the hypoperfusion seen in the penumbra

Table 2
Comparison of CVR metrics in regions of NAWM that progressed to WMH against other tissue types. Values are given as mean (SD). ssCVR comparisons were made using Friedman test with Dunn's correction for multiple comparison while comparisons involving τ were made using repeated measures one-way ANOVA with Bonferroni correction.

	Grey matter	All NAWM	Pre-existing WMH	Baseline NAWM that progressed to WMH
ssCVR [% BOLD/mmHg]	0.32	0.17	0.11	0.09
	(0.07)	(0.06)[*]	(0.06)[*+]	(0.08)[*+]
τ [s]	23.50	35.62	50.25	46.02
	(7.47)	(9.30)[*]	(11.52)[*+]	(15.86)[*+]

[*] Denotes significance vs. grey matter ($P < 0.01$).
[+] Denotes significance vs. all NAWM ($P < 0.01$). No significant differences were observed between pre-existing WMH and NAWM that progressed to WMHs.

Table 3
Comparison of CVR metrics in pre-existing white matter hyperintensities and contralateral homologous white matter regions. Values are given as mean (SD).

	Pre-existing WMHs	Contralateral NAWM
ssCVR [% BOLD/mmHg]	0.11 (0.06)	0.18 (0.06)[*]
τ [s]	36.95 (7.59)	34.72 (8.01)[*]

[*] Denotes significance against pre-existing WMHs ($P < 0.001$) using Wilcoxon matched-pairs signed ranks test for CVR and ssCVR and two-tailed paired t-test for τ.

of large infarcts also displays prolonged time-dependent metrics measured with dynamic susceptibility contrast perfusion imaging (Campbell et al., 2012; Srinivasan et al., 2006). These include mean transit time, time-to-peak of the tissue-concentration curve, and time-to-peak of the deconvolved tissue residue function. Prolonged τ has also been reported in patients with unilateral large artery steno-occlusive disease (Poublanc et al., 2015). Together these findings are consistent with the notion that dysregulation of cerebral blood flow control and chronic low-grade ischemia play a causative role in WMH progression.

Some previous studies have suggested that differences between WMH and NAWM are due to regional variability in metabolic demand. Indeed, blood flow reductions in WMHs found in a study using 18 F fluoromethane positron emission tomography (Herholz et al., 1990) were thought to result from the lower metabolic demands of the cortex rendered electrophysiologically isolated by subjacent zones of degenerated white matter tissue. According to this notion, hypoperfusion may not be involved in the pathophysiology of WMHs. Also, hemodynamically significant extracranial carotid stenosis has been shown not to correlate with the presence of ipsilateral WMHs (Fazekas et al., 1988) although WMH progression has been shown to correlate with significant carotid stenosis that advanced to complete occlusion (Ylikoski et al., 1993). In spite of these findings, we have shown a reduction in steady-state CVR, and prolonged τ in WMHs compared to the contralateral homologous NAWM, suggesting that abnormal vascular responses are an etiologic mechanism of WMH progression.

A strength and unique feature of our study is the ability to accurately control $P_{ET}CO_2$ throughout the experiment. The magnitude of the stimulus may determine the distribution of blood flow during steal physiology (Sobczyk et al., 2014). All subjects had an abrupt 10 mmHg change in $P_{ET}CO_2$ (within 1-2 breaths) from an average baseline of 40 mmHg, providing a consistent stimulus between subjects. Consistency in stimulus magnitude reduces the uncertainty of test-to-test CVR variability. The time profile of the stimulus, which in our study was 10 s, allowed us to measure a range of response times 10 s and longer. Vascular response times faster than the changes in the arterial PCO2 (which are seldom known) cannot be measured.
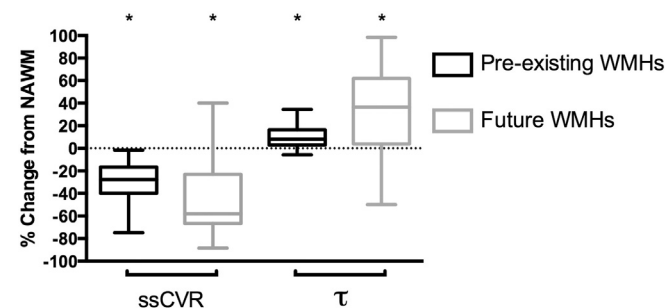

Fig. 3. Comparison of cerebrovascular metrics in regions of pre-existing and future WMHs. All values are given as % change from contralateral NAWM and assessed on baseline MRI scans. Values for future WMHs are made in the NAWM on the baseline scan (before the progression into overt WMH). ssCVR are significantly lower and τ is significantly higher in pre-existing and future WMHs compared to NAWM. * denotes significance compared to NAWM ($P < 0.01$). Bars indicate minimum and maximum, boxes indicate the interquartile range (25th to 75th percentile) and the line within each box indicates the median.

4.1. Limitations

We assumed that the BOLD signal was a surrogate measure of CBF. Although the BOLD signal has a complex dependency upon CBF, hematocrit, cerebral blood volume, and cerebral metabolic rate for oxygen (Ogawa et al., 1993), CBF measured with arterial spin labeling has demonstrated a linear relationship with the BOLD signal in the $P_{ET}CO_2$ range of 40 to 50 mmHg (Tancredi and Hoge, 2013). Mandell et al. (2008) have also previously shown a highly correlated BOLD signal response to hypercapnia compared with CBF measurements obtained with ASL in patients with large artery steno-occlusive disease.

Our measurements also assume that changes in the arterial partial pressure of CO_2 do not influence $CMRO_2$. This assumption is supported by experiments showing that increases in CBF through vasodilation produce very little or no increases in $CMRO_2$ (Sokoloff, 1981).

5. Conclusion

In summary, these experiments show that both the magnitude and the speed of the vascular response to a CO_2 challenge are reduced in NAWM that progresses to WMH. This is the first report to show that abnormal dynamic cerebrovascular response precedes the development of WMH.

Author contributions statement

All authors agreed to be accountable with regards to the accuracy and integrity of the work. All authors have critically revised the manuscript and approved of the final manuscript to be published. Study concept and design: K.S., A.P.C., D.M.M., J.D., J.A.F., S.E.B., & D.J.M. Acquisition of data: K.S., & O.S. Data analysis and interpretation: K.S., B.P., J.C., J.P., A.P.C., D.M.M., L.V., J.D., J.A.F., S.E.B., & D.J.M. Statistical plan and analysis: K.S., J.C., & A.P.C. Obtained funding: L.V., J.A.F., S.E.B., & D.J.M.

Disclosure

K. Sam, K. Holmes, A.P. Crawley, J. Poublanc, J. Conklin, O. Sobczyk, J. Duffin, and D.M. Mandell declare no disclosures. Dr. Fisher is a coinventor of the RespirAct, a device used in this study. He also holds shares and serves as a director of Thornhill Research Inc., a University of Toronto/University Health Network-related company, which retains an ownership position and will receive royalties should the RespirAct become a commercial product. Dr. Mikulis is a co-inventor of the RespirAct, a device used in this study and holds a minor equity position in Thornhill Research Inc. and has received research support from GE Healthcare, Siemens, Toshiba, and the Ontario Research Fund. Dr. Black has received compensation in the past 2 years for ad hoc consulting with Boehringer Ingelheim and Novartis and for honoraria from the Rehabilitation Institute of Chicago and Heart and Stroke Richard Lewar Centre of Excellence in Cardiovascular Research, Eisai Korea, and Novartis. Her research unit is receiving research funding from Roche, GE Healthcare, Lilly Avid, Pfizer, Lundbeck, and Transition Therapeutics. Dr. Black also receives research funding from CIHR, NIH, Heart and Stroke Foundation of Canada,

References

Blahak, C., Baezner, H., Pantoni, L., et al., 2009. Deep frontal and periventricular age related white matter changes but not basal ganglia and infratentorial hyperintensities are associated with falls: cross sectional results from the LADIS study. J. Neurol. Neurosurg. Psychiatry 80 (6), 608–613.

Campbell, B.C., Christensen, S., Levi, C.R., et al., 2012. Comparison of computed tomography perfusion and magnetic resonance imaging perfusion-diffusion mismatch in ischemic stroke. Stroke 43 (10), 2648–2653.

Cox, R.W., 1996. AFNI: software for analysis and visualization of functional magnetic resonance neuroimages. Comput. Biomed. Res. 29 (3), 162–173.

Englund, E., 2002. Neuropathology of white matter lesions in vascular cognitive impairment. Cerebrovasc. Dis. 13 (Suppl. 2), 11–15.

Fazekas, F., Niederkorn, K., Schmidt, R., et al., 1988. White matter signal abnormalities in normal individuals: correlation with carotid ultrasonography, cerebral blood flow measurements, and cerebrovascular risk factors. Stroke 19 (10), 1285–1288.

Fierstra, J., Sobczyk, O., Battisti-Charbonney, A., et al., 2013. Measuring cerebrovascular reactivity: what stimulus to use? J. Physiol. 591 (23), 5809–5821.

Fisher, J.A., 2016. The CO2 stimulus for cerebrovascular reactivity: fixing inspired concentrations vs. targeting end-tidal partial pressures. J. Cereb. Blood Flow Metab.

Greensburg, J.H., Reivich, M., 1977. Response time of cerebral arterioles to alterations in extravascular fluid pH. Microvasc. Res. 14 (3), 383–393.

Gunning-Dixon, F.M., Raz, N., 2000. The cognitive correlates of white matter abnormalities in normal aging: a quantitative review. Neuropsychology 14 (2), 224–232.

Han, J.S., Mikulis, D.J., Mardimae, A., et al., 2011. Measurement of cerebrovascular reactivity in pediatric patients with cerebral vasculopathy using blood oxygen level-dependent MRI. Stroke 42 (5), 1261–1269.

Herholz, K., Heindel, W., Rackl, A., et al., 1990. Regional cerebral blood flow in patients with leuko-araiosis and atherosclerotic carotid artery disease. Arch. Neurol. 47 (4), 392–396.

Ishii, N., Nishihara, Y., Imamura, T., 1986. Why do frontal lobe symptoms predominate in vascular dementia with lacunes? Neurology 36 (3), 340–345.

Launer, L.J., Berger, K., Breteler, M.M., et al., 2006. Regional variability in the prevalence of cerebral white matter lesions: an MRI study in 9 European countries (CASCADE). Neuroepidemiology 26 (1), 23–29.

Liao, D., Cooper, L., Cai, J., et al., 1997. The prevalence and severity of white matter lesions, their relationship with age, ethnicity, gender, and cardiovascular disease risk factors: the ARIC study. Neuroepidemiology 16 (3), 149–162.

Mandell, D.M., Han, J.S., Poublanc, J., et al., 2008. Mapping cerebrovascular reactivity using blood oxygen level-dependent MRI in patients with arterial steno-occlusive disease: comparison with arterial spin labeling MRI. Stroke 39 (7), 2021–2028.

Ogawa, S., Menon, R.S., Tank, D.W., et al., 1993. Functional brain mapping by blood oxygenation level-dependent contrast magnetic resonance imaging. A comparison of signal characteristics with a biophysical model. Biophys. J. 64 (3), 803–812.

Poublanc, J., Crawley, A.P., Sobczyk, O., et al., 2015. Measuring cerebrovascular reactivity: the dynamic response to a step hypercapnic stimulus. J. Cereb. Blood Flow Metab.

Ramirez, J., Gibson, E., Quddus, A., et al., 2011. Lesion explorer: a comprehensive segmentation and parcellation package to obtain regional volumetrics for subcortical hyperintensities and intracranial tissue. NeuroImage 54 (2), 963–973.

Ramirez, J., Scott, C.J., McNeely, A.A., et al., 2014. Lesion explorer: a video-guided, standardized protocol for accurate and reliable MRI-derived volumetrics in Alzheimer's disease and normal elderly. J. Vis. Exp. 86.

Roman, G.C., 1987. Senile dementia of the Binswanger type. A vascular form of dementia in the elderly. JAMA 258 (13), 1782–1788.

Sam, K., Poublanc, J., Sobczyk, O., et al., 2015. Assessing the effect of unilateral cerebral revascularisation on the vascular reactivity of the non-intervened hemisphere: a retrospective observational study. BMJ Open 5 (2), e006014.

Schmidt, R., Schmidt, H., Kapeller, P., et al., 2002. The natural course of MRI white matter hyperintensities. J. Neurol. Sci. 203–204, 253–257.

Shapiro, E., Wasserman, A.J., Patterson Jr., J.L., 1965. Human cerebrovascular response time to elevation of arterial carbon dioxide tension. Arch. Neurol. 13, 130–138.

Slessarev, M., Han, J., Mardimae, A., et al., 2007. Prospective targeting and control of end-tidal CO2 and O2 concentrations. J. Physiol. 581 (3), 1207–1219.

Sobczyk, O., Battisti-Charbonney, A., Fierstra, J., et al., 2014. A conceptual model for CO(2)-induced redistribution of cerebral blood flow with experimental confirmation using BOLD MRI. NeuroImage 92, 56–68.

Sobczyk, O., Battisti-Charbonney, A., Poublanc, J., et al., 2015. Assessing cerebrovascular reactivity abnormality by comparison to a reference atlas. J. Cereb. Blood Flow Metab. 35 (2), 213–220.

Sokoloff, L., 1981. Relationships among local functional activity, energy metabolism, and blood flow in the central nervous system. Fed. Proc. 40 (8), 2311–2316.

Spano, V.R., Mandell, D.M., Poublanc, J., et al., 2013. CO2 blood oxygen level-dependent MR mapping of cerebrovascular reserve in a clinical population: safety, tolerability, and technical feasibility. Radiology 266 (2), 592–598.

Srinivasan, A., Goyal, M., Al Azri, F., Lum, C., 2006. State-of-the-art imaging of acute stroke. Radiographics 26 (Suppl. 1), S75–S95.

Tancredi, F.B., Hoge, R.D., 2013. Comparison of cerebral vascular reactivity measures obtained using breath-holding and CO2 inhalation. J. Cereb. Blood Flow Metab. 33 (7), 1066–1074.

Uh, J., Yezhuvath, U., Cheng, Y., Lu, H., 2010. In vivo vascular hallmarks of diffuse leukoaraiosis. J. Magn. Reson. Imaging 32 (1), 184–190.

Verdelho, A., Madureira, S., Moleiro, C., et al., 2010. White matter changes and diabetes predict cognitive decline in the elderly: the LADIS study. Neurology 75 (2), 160–167.

Wardlaw, J.M., Smith, E.E., Biessels, G.J., et al., 2013. Neuroimaging standards for research into small vessel disease and its contribution to ageing and neurodegeneration. Lancet Neurol. 12 (8), 822–838.

Whitman, G.T., Tang, Y., Lin, A., Baloh, R.W., 2001. A prospective study of cerebral white matter abnormalities in older people with gait dysfunction. Neurology 57 (6), 990–994.

Ylikoski, R., Ylikoski, A., Erkinjuntti, T., et al., 1993. White matter changes in healthy elderly persons correlate with attention and speed of mental processing. Arch. Neurol. 50 (8), 818–824.